Thermal expansion and phonon anharmonicity of cuprite studied by inelastic neutron scattering and *ab initio* calculations

C. N. Saunders, D. S. Kim, O. Hellman, H. L. Smith, N. J. Weadock, S. T. Omelchenko, G. E. Granroth, C. M. Bernal-Choban, S. H. Lohaus, D. L. Abernathy, and B. Fultz

Phys. Rev. B **105**, 174308 — Published 31 May 2022

DOI: 10.1103/PhysRevB.105.174308

Phonon Anharmonicity of Cuprite (Cu_2O)

C. N. Saunders,[1,*] D. S. Kim,[2] O. Hellman,[3,4] H. L. Smith,[5] N. J. Weadock,[6] S. T. Omelchenko,[1] G. E. Granroth,[7] C. M. Bernal-Choban,[1] S. H. Lohaus,[1] D. L. Abernathy,[7] and B. Fultz[1,†]

[1]*Department of Applied Physics and Materials Science, California Institute of Technology, Pasadena, California 91125, USA*
[2]*Department of Materials Science and Engineering, Massachusetts Institute of Technology, Cambridge, Massachusetts 02139, USA*
[3]*Department of Physics, Chemistry, and Biology (IFM), Linkping University, SE-581 83 Linkping, Sweden*
[4]*Department of Molecular Chemistry and Material Science, Weizmann Institute of Science, Rehovot 76100, Israel*
[5]*Department of Physics and Astronomy, Swarthmore College, Swarthmore, PA 19081, USA*
[6]*Department of Chemical and Biological Engineering, University of Colorado Boulder, Boulder, CO, 80309, USA*
[7]*Neutron Scattering Division, Oak Ridge National Laboratory, Oak Ridge, Tennessee 37831, USA*

(Dated: May 10, 2022)

Inelastic neutron scattering measurements were performed with a time-of-flight chopper spectrometer to obtain phonons in all parts of the Brillouin zone of a single crystal of cuprite, Cu_2O. We reduced the experimental data to phonon dispersions in the high symmetry directions, and changes between 10 K and 300 K are reported. This work shows *ab initio* quasiharmonic (QH) and anharmonic (AH) calculations of phonon dispersions. We performed all AH calculations with a temperature-dependent effective potential method. Both QH and AH calculations account for the small negative thermal expansion of cuprite at low temperatures. However, the measured temperature-dependent phonon behavior was predicted more accurately with the AH calculations than the QH. Nevertheless, at 300 K, the cubic anharmonicity used in the present work did not entirely account for the experimental phonon dispersions in cuprite.

I. INTRODUCTION

Cuprite, Cu_2O, (Fig. 1) is one of the first known semiconductors [1, 2]. It has applications in photovoltaics [3, 4], nanoelectronics [5], thermoelectrics [6], spintronics [7], and catalysis [8, 9]. Cuprite has small coefficient of thermal expansion that is negative at low temperatures but becomes positive above 300 K. The coefficient of volumetric thermal expansion, $\beta = \frac{1}{V}\frac{\partial V}{\partial T}$ (V is volume and T is temperature), is explained with thermodynamics from a balance between the internal energy, U, and the entropy, S. At finite temperatures, the primary contributions to U and S are the elastic energy ($U_{\rm el}$) and the vibrational entropy of phonons ($S_{\rm vib}$). Using this approximation, the total free energy, $F = U_{\rm el} - TS_{\rm vib}$, is minimized when reductions in the phonon frequencies with volume (and temperature) cause a larger $S_{\rm vib}$. These changes counteract the energy penalty from $U_{\rm el}$ during thermal expansion.

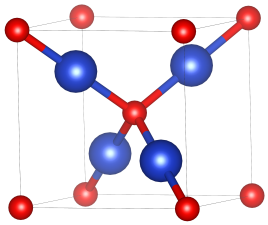

FIG. 1. Unit cell of Cu_2O. Copper (Cu) atoms are shown in blue and oxygen (O) atoms in red. There is a linear arrangement of O-Cu-O as the $3z^2 - r^2$ orbitals of copper make chemical bonds with the sp^3 orbitals of oxygen [10].

Spectroscopies to study phonons include inelastic neutron, inelastic X-ray, and Raman methods. All of these methods have been used to study phonons in cuprite [11–30]. Inelastic neutron scattering (INS) experiments with triple-axis spectrometers measure energy spectra of phonons at single points in crystal momentum, $\vec{q}$. Thermophysical properties such as thermal expansion and the temperature dependence of elastic constants depend on the phonon frequencies at all $\vec{q}$-points in the first Brillouin zone. New methods of INS on single crystals at pulsed neutron sources can provide such detailed information [31, 32]. Measurements of all phonons in a crystal allow testing or microscopic models of thermophysical properties.

The free energy $F_{\rm vib}$ in the anharmonic (AH) theory used here is

$$F_{\rm vib}(V,T) = U_0(V,T) + \sum_{\vec{q},s}\left[\frac{\hbar\omega_{\vec{q},s}(V,T)}{2} + k_BT\ln\left(1 - e^{-\frac{\hbar\omega_{\vec{q},s}(V,T)}{k_BT}}\right)\right], \quad (1)$$

where the phonon frequencies, $\omega_{\vec{q},s}$ (s is a branch index),

* clairenicolesaunders@gmail.com
† btf@caltech.edu

depend on both V and T. An explicit dependence on T is essential for AH models. The quasiharmonic (QH) vibrational Helmholtz free energy contribution, $F_{\rm vib}$, depends explicitly on V, and effects of T are only through thermal expansion, $\omega_{\vec{q},s}(V(T))$, rather than $\omega_{\vec{q},s}(V,T)$ for AH theory. Phonons in materials can be modeled or interpreted with QH or AH theories [33].

The present study identifies the microscopic physics of the individual phonon modes that contribute to the macroscopic thermal expansion. We do this by calculating individual phonon contributions to $F_{\rm vib}$ with both QH and AH theory and comparing the thermal trends of the calculated phonons to new phonon measurements by INS on cuprite at 10 K and 300 K. The net volume change of cuprite from thermal expansion between 10 K and 300 K is small, so QH calculations predict phonon shifts that are nearly zero. On the other hand, experiment and AH calculations give thermal shifts and broadening phonons, especially optical modes. However, we expect the low-frequency acoustic modes to be more pertinent to the NTE at low temperatures. We found small but measurable changes in the acoustic phonons between 10 K and 300 K. Closer examination shows that QH theory predicts changes in both magnitude and sign of the thermal shifts of the lowest acoustic branch at different $\vec{q}$. On the other hand, AH theory and experiment show that this entire branch undergoes a thermal shift that is nearly the same at all $\vec{q}$.

II. EXPERIMENT

A. Powder

INS measurements were performed first on a 20 g powder of Cu_2O with the time of flight (TOF) Wide Angular-Range Chopper Spectrometer (ARCS) [31] at the Spallation Neutron Source (SNS) at Oak Ridge National Laboratory (ORNL) [34]. The incident energy was 120 meV, and sample temperatures were 5 K and 300 K. Using the software packages Mantid and Multiphonon, we reduced the data to phonon density of states (DOS) curves [35, 36]. The reduction included subtractions of an empty aluminum can background and a multiphonon correction.

B. Single Crystal

Further INS measurements used ARCS to perform measurements on a single-crystal of cuprite. The [100] oriented single crystal was grown at the Joint Center for Artificial Photosynthesis at Caltech in an optical furnace with the float zone method [37] with 99.999% Cu rods from Alfa Aesar. The crystal was a cylinder of 50 mm in height and 7 mm in diameter, suspended in a platinum holder for all measurements. See Supplemental Material at [URL will be inserted by the production group] for images of the crystal and mount (see, also, references [38–44] therein).

For 10 K measurements, the crystal was in an aluminum canister within a closed-cycle helium refrigerator. TOF neutron spectra were acquired at 152 individual angles of the crystal in increments of 0.5°, about the vertical axis. For 300 K measurements, we mounted the crystal in a low-background electrical resistance vacuum furnace [45]. Measurements at 300 K used 201 angles in increments of 0.5°. The incident energy for all single-crystal measurements was 110 meV. An oscillating radial collimator suppressed multiple scattering and background.

To reduce the single crystal data to obtain the four-dimensional $S(\vec{Q},\varepsilon)$, we used Mantid. An additional analysis assessed the data statistics and alignment. Following crystal symmetry, we folded the data from high $\vec{Q}$ into the irreducible wedge in the first Brillouin zone. An averaged multiphonon scattering correction was subtracted from the data, and spectral weights were thermal factor corrected. The results of our analysis appear in Fig. 2 with further details of data post-processing available in the Supplemental.

III. COMPUTATION

The Vienna Ab Initio Simulation Package (VASP) was used for all *ab initio* DFT calculations [46–49] with plane wave basis sets, projector augmented wave (PAW) pseudopotentials [50] and the SCAN meta-GGA exchange correlation functional [51]. All calculations used 3×3×3 supercells containing 162 atoms, a 2×2×2 k-grid, and a kinetic energy cutoff of 600 eV. The supercell configurations for calculations were generated with the stochastic Temperature Dependent Effective Potential (sTDEP) method or PHONOPY [52]. For further details on calculation parameters see Supplemental.

We found the equilibrium volume for each temperature by minimizing the Helmholtz free energy, which included electronic and phononic contributions, for five volumes (±1.5%, ±3.0%, and the 0 K equilibrium volume) with respect to volume. For each volume, we performed QH calculations with PHONOPY. All QH calculations used the finite displacement method. AH calculations used the sTDEP package [53–55]. Finally, we fit the Helmholtz free energy to the Birch-Murnaghan equation of state. The minimum of this function provided the equilibrium volume at the temperature of interest.

Anharmonic effects on lattice parameter and on phonons are accounted for in $\mathrm{U}_0(T,V)$ and $\omega_{\vec{q},s}(T,V)$. The expression for $\mathrm{U}_0(T,V)$ in our AH thermal expansion calculations is:

$$U_0(V,T) = \left\langle U_{\rm BO}(V,T) - \frac{1}{2}\sum_{ij}\sum_{\alpha\beta}\Phi_{ij}^{\alpha\beta}u_i^{\alpha}u_j^{\beta} \right\rangle \quad (2)$$

where $U_{\rm BO}(T,V)$ is the Born-Oppenheimer potential energy from sampling the surface and $\Phi_{ij}^{\alpha\beta}$ are forces that are matched between the actual system and with our

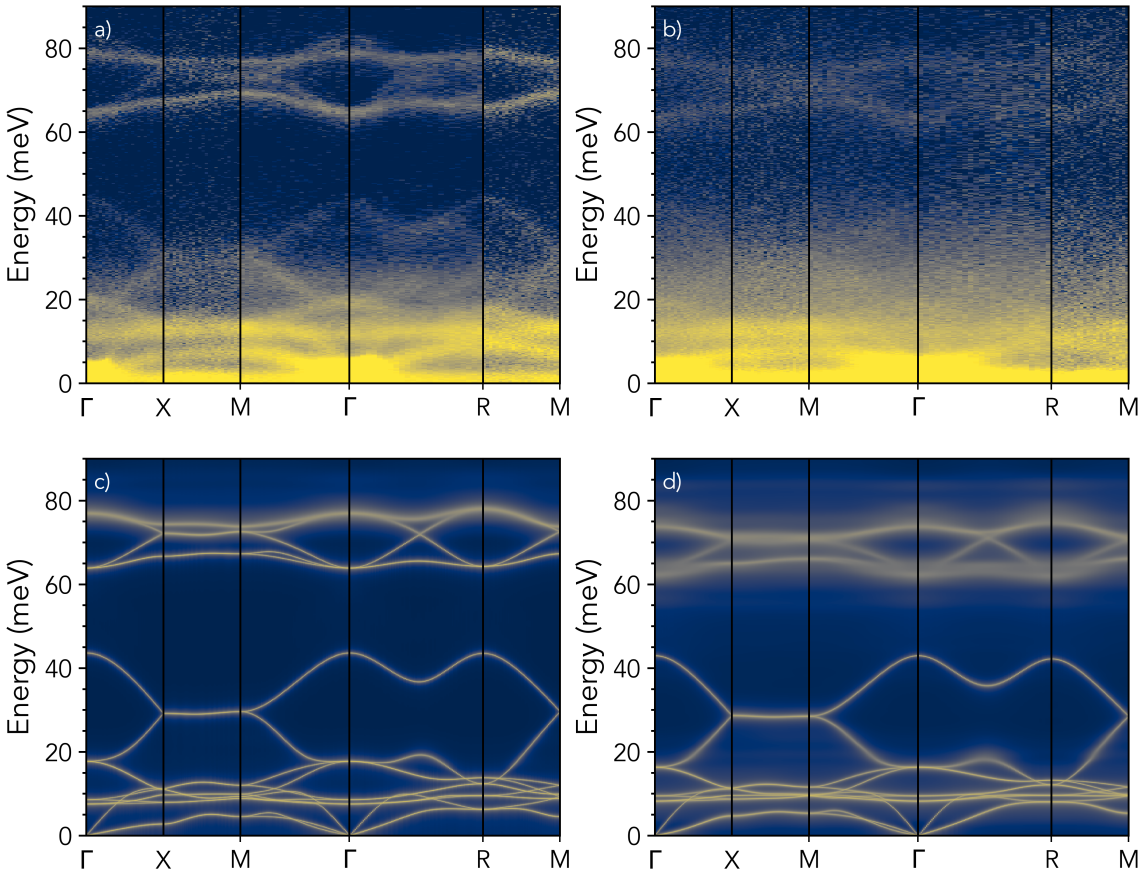

FIG. 2. Phonon dispersions along high symmetry directions measured by INS at a) 10 K and b) 300 K. Phonon dispersions calculated by sTDEP at c) 10 K and d) 300 K.

model Hamiltonian. The u_i^α and u_j^β are Cartesian components of the displacements of atoms i and j. Accounting for third-order terms for phonon self-energies

$$U_0(V,T) = \left\langle U_{\mathrm{BO}}(V,T) - \frac{1}{2!}\sum_{ij}\sum_{\alpha\beta}\Phi_{ij}^{\alpha\beta}u_i^\alpha u_j^\beta - \frac{1}{3!}\sum_{ijk}\sum_{\alpha\beta\gamma}\Phi_{ijk}^{\alpha\beta\gamma}u_i^\alpha u_j^\beta u_k^\gamma \right\rangle . \tag{3}$$

After obtaining the lattice parameter, we calculated the phonon dispersions and self-energy at that volume.

Previous studies of lattice dynamics and the NTE of cuprite used the QH approximation. In QH theory, each phonon mode s with corresponding angular frequency $\omega_{\vec{q},s}$ depends directly on the volume through the mode Grüneisen parameter, $\gamma_{\vec{q},s}$, at a given wavevector $\vec{q}$,

$$\gamma_{\vec{q},s}(V) = -\frac{V}{\omega_{\vec{q},s}(V)}\,\frac{\partial\omega_{\vec{q},s}(V)}{\partial V}. \tag{4}$$

Equation 4 predicts thermal shifts of individual phonon frequencies. An average γ, where each $\gamma_{\vec{q},s}$, is weighted by the contribution of phonon s to the heat capacity,

predicts the macroscopic thermal expansion. Average phonon frequencies decrease for positive values of γ as volume increases. This decrease in $\omega_{\vec{q},s}$ contributes positively to the vibrational entropy, S_{vib}, and lowers the QH vibrational Helmholtz free energy, F^{QH}.

For AH computations, where third-order force constants are available [56], the mode Grüneisen parameters for a mode with frequency $\omega_{\vec{q},s}$ is:

$$\gamma_{\vec{q},s}(V,T) = -\frac{V}{6\omega_{\vec{q},s}(V,T)^2} \sum_{ijk\alpha\beta\gamma} \frac{\epsilon^{i\alpha\dagger}_{\vec{q},s}\epsilon^{j\beta}_{\vec{q},s}}{\sqrt{m_i m_j}} r^{\gamma}_{k} \Phi^{\alpha\beta\gamma}_{ijk} e^{\vec{q}\cdot\vec{r}_j}. \tag{5}$$

Here $\Phi^{\alpha\beta\gamma}_{ijk}$ is the cubic anharmonicity tensor with Cartesian indices α, β, γ. ϵ is the polarization eigenvector, and atomic position and mass are designed by $\vec{r}$ and m, respectively. Equation 5 offers an advantage over Eq. 4 because it is not divergent when the thermal expansion is zero, so the mode Grüneisen parameters were calculated using Eq. 5. All calculations were performed in sTDEP using the third order force constants.

The calculated phonon self-energy gives phonon spectra with thermal shifts and finite linewidths. Calculations of this include terms to the third power of atom displacements (cubic anharmonicity) [57, 58]. We performed AH calculations of the self-energy with sTDEP. By solving a dynamical matrix, we obtained phonon frequencies. For a given third-order force constant, $\Phi_{ss's''}$, we calculated and adjusted the phonon self-energy with the real Δ and imaginary Γ corrections to the phonon self-energy. The imaginary correction is:

$$\Gamma^{\vec{q}\vec{q}'\vec{q}''}_{ss's''}(V,T) = \frac{\hbar\pi}{16} \sum_{ss's''} \left|\Phi^{\vec{q}\vec{q}'\vec{q}''}_{ss's''}\right|^2 (n_{\vec{q}',s'} + n_{\vec{q}'',s''} + 1) \times \delta\left(\Omega - \omega_{\vec{q}',s'} - \omega_{\vec{q}'',s''}\right) \tag{6}$$

$$+ \left(n_{\vec{q}',s'} - n_{\vec{q}'',s''}\right) \left[\delta\left(\Omega - \omega_{\vec{q}',s'} + \omega_{\vec{q}'',s''}\right) - \delta\left(\Omega + \omega_{\vec{q}',s'} - \omega_{\vec{q}'',s''}\right)\right] \tag{7}$$

where $\hbar\Omega$ is a probing energy, $\omega^2_{\vec{q},s}$ are the eigenvalues of the dynamical matrix, and n are the occupancy factors. The three-phonon matrix component can be written as:

$$\Phi^{\vec{q}\vec{q}'\vec{q}''}_{ss's''} = \sum_{ijk}\sum_{\alpha\beta\gamma} \frac{\epsilon^{i\alpha}_{s}\epsilon^{j\beta}_{s'}\epsilon^{k\gamma}_{s''}}{\sqrt{m_i m_j m_k}\sqrt{\omega_{\vec{q},s}\omega_{\vec{q}',s'}\omega_{\vec{q}'',s''}}} \Phi^{\alpha\beta\gamma}_{ijk} e^{i\left(\vec{q}\cdot\vec{r}_i + \vec{q}'\cdot\vec{r}_j + \vec{q}''\cdot\vec{r}_k\right)} \tag{8}$$

where the primes help identify the three-phonon interactions. Remaining indices are defined after Eq. 5.

The real part of the phonon self-energy correction is obtained from the Kramers-Kronig transform:

$$\Delta_{\vec{q},s}(\Omega_{\vec{q},s}) = \frac{1}{\pi}\int \frac{\Gamma(\omega_{\vec{q},s})}{\omega_{\vec{q},s} - \Omega} d\omega_{\vec{q},s} \tag{9}$$

Large deviations of $\Delta_{\vec{q},s}(\Omega_{\vec{q},s})$ from a Lorentzian functions suggest a high degree of anharmonicity.

In the QH approximation, Eq. 1 reduces to:

$$F^{\text{QH}}_{\text{vib}}(V,T) = U_0(V) \tag{10}$$
$$+ \sum_{\vec{q},s}\left[\frac{\hbar\omega_{\vec{q},s}(V)}{2} + k_B T \ln\left(1 - e^{-\frac{\hbar\omega_{\vec{q},s}(V)}{k_B T}}\right)\right].$$

In the QH approximation, phonon frequencies and ground state energy do not have explicit temperature dependence, but $V = V(T)$ with thermal expansion.

IV. RESULTS

Figure 2 shows phonon spectra from INS measurements and AH calculations projected on the high-symmetry crystallographic directions. Figures 2a,b) shows the folded experimental data from the single crystal at 10 and 300 K, respectively, and Figs. 2c,d) show the corresponding AH sTDEP calculations. The main features and energies of the calculated and measured intensities agree. Both calculated and measured data show softening of the high-energy optical modes. However, the calculated softening of these modes is larger than the experimental results. Below 45 meV, small changes in the calculated and measured dispersions follow the same thermal trends.

Figure 3b) shows the phonon partial DOS curves for Cu-atoms and O-atoms in cuprite, calculated by sTDEP. The O-atoms dominate the spectral weight in the high-energy modes between 65 and 80 meV, and Cu-atoms dominate below 45 meV. Their sum agrees with the ex-

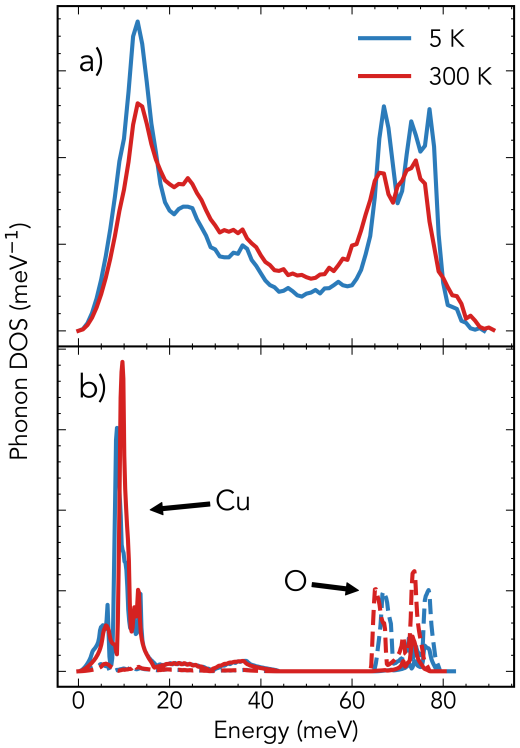

FIG. 3. a) Phonon DOS from INS measurements on powdered cuprite. b) Phonon partial DOS from sTDEP calculations using second order terms at 10 K and 300 K. Solid curves are Cu-atoms, dashed are O-atoms.

perimental spectra from INS measurements shown in Fig. 3a), without neutron-weight corrections.

Figure 4 compares experimental cuts taken at single $\vec{q}$-points along high symmetry paths to cuts calculated with sTDEP and to energies from PHONOPY. The AH sTDEP results show thermal shifts, but the QH PHONOPY calculations display no discernible changes with the temperature on the scale of Fig. 4. Grüneisen parameters from sTDEP with Eq. 5 are shown in Figs. 5a, c) at different temperatures. These Grüneisen parameters are in good agreement with prior QH calculations and experimental results [59]. The plots are color-coded, so the Grüneisen parameters for each mode correspond to the same color mode in the dispersions in Fig. 5 b,d. Many of the low-energy dispersions have negative Grüneisen parameters, including the low-energy transverse acoustic (TA) modes that are useful for explaining the negative thermal expansion in QH theory. The high-energy optical modes have positive Grüneisen parameters, but these are similar to the Grüneisen parameters of other phonon branches. Modes with similar Grüneisen parameters are predicted by QH theory to have similar thermal shifts. The real and imaginary parts of the phonon self-energy at the point $\vec{Q} = (0.25, 0.25, 0.00)$ appear in Fig. 6, colored in correspondence with their phonon branches in Fig. 5. Significant deviations from the harmonic self-energy for the optical modes with energies above 70 meV, show that these modes are more AH than the other modes. There are also substantial AH effects from cubic anharmonicity for the lower energy optical modes around 40 meV. Comparing the partial density of states to the self-energies shows that the displacements of oxygen atoms dominate these AH modes.

Figure 7 shows the percentage change in lattice parameter of cuprite versus temperature, referenced to a nominal 0 K. Panel a) compares the sTDEP lattice parameter to experimental results, and panel b) compares it to our QH calculations and other QH calculations in the literature. Both QH and AH calculations below 250 K reproduce the measured negative thermal expansion. However, the thermal expansion coefficient in this region is small, no larger than -2.4×10^{-6}/K, and is zero near 250 K.

V. DISCUSSION

The AH sTDEP calculations better predict the measured effect of temperature on cuprite phonons than by QH PHONOPY calculations, as seen in the energy cuts of Fig. 4. For cuprite, Grüneisen parameters from sTDEP and QH calculations are essentially the same [59]. In the QH approximation, phonon shifts follow the $\vec{q}$-dependence of the Grüneisen parameters shown in Fig. 5, which is not the thermal trend of the phonon branches. There are two key differences. First, the phonon frequencies depend solely on volume in QH theory, so it predicts a negligible difference between calculated dispersions at 10 K and 300 K. While the thermal shifts are small, they are measurable and larger than predicted by QH calculations. A second problem appears in Fig. 5. For the low TA branch at the X point, the Grüneisen parameter is –4, whereas it is approximately +5 at the R point. However, the entire low TA branch in the experimental results (and sTDEP) in Fig. 2 shifts upwards in energy with temperature between 10 K and 300 K as shown in Fig. 4. There are no observable differences in the behavior at the X-point or R-point. The Grüneisen parameters for the low-energy optical branches also change signs at different $\vec{q}$, but the branches from sTDEP have simple behavior. For the modes below 11 meV shifts up with temperature, and for those above 11 meV shifts down with temperature.

Previous studies of cuprite showed the success of QH theory for predicting thermal expansion [59, 61–64], and some studies included results on phonon dynamics [61, 62, 65]. We find similar success with the QH theory for thermal expansion and find similar success with the AH theory. These results seem similar to a previous study on the thermal expansion of silicon, another small NTE material, which showed that AH effects dominate over QH effects for thermal phonon shifts at low temperatures

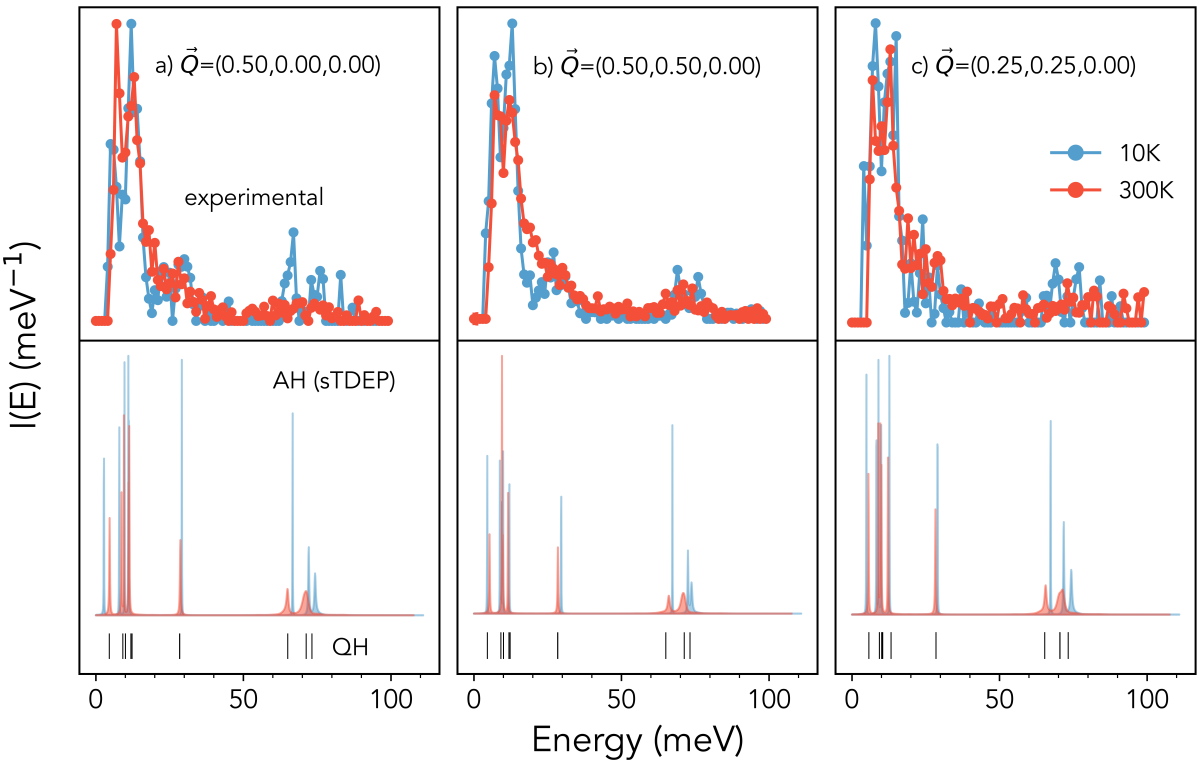

FIG. 4. Energy spectra at three values of $\vec{Q}$ at 10 K (blue) and 300 K (red). **a**) Energy cut at X-point for experimental (top panel), AH calculations (lower panel), and QH calculation (lower panel, black lines) at labeled temperatures. **b**) Energy cut at M-point. **c**) Energy cut at the halfway point between the high symmetry points X and M. The color specifies the experimental and AH data temperature. Both temperatures of the QH data are denoted by black at the bottom because there is no discernible change of QH phonons between 10 K and 300 K.

[32, 66].

The thermal expansion from Eq. 1 depends only on the temperature dependence of U through the electronic energy, and the temperature dependence of S through the phonon frequencies, $\mathrm{d}\omega_{\vec{q},s}/\mathrm{d}T$. With anharmonicity, $\omega_{\vec{q},s}$ depends independently on both T and V. In quasi-harmonicity, we assume $\omega_{\vec{q},s}(V(T))$ so all effects from T originate solely with $\Delta V = \beta T V$. The QH approximation gives generally good results for thermal expansion, as shown in Fig. 7, even though it does not reliably predict the $\mathrm{d}\omega_{\vec{q},s}/\mathrm{d}T$ (for many phonons, the $\mathrm{d}\omega_{\vec{q},s}/\mathrm{d}T$ in the QH approximation has the wrong sign). With its prediction of tiny shifts in phonon frequencies between 10 K and 300 K, it is difficult to pinpoint why the QH approximation might successfully predict the thermal expansion. Perhaps its success originates from a fortuitous cancellation of errors.

Three-phonon processes are subject to kinematic constraints. The energy constraint requires pairs of lower energy phonons to add their energy to create a higher-energy phonon. This process alters the self energies, and Fig. 6 shows peaks at some energies where the self-energy corrections are significant. For example, at 10 K, most of the 3-phonon processes involve down-conversion and dominate the high energy optical modes at 300 K (the self-energy corrections above 40 meV are similar at 10 and 300 K). Figure 6 shows that other self-energy corrections are becoming larger at 300 K than 10 K. Examination of the self-energy corrections and the phonon partial DOS curves of Fig. 3 shows a large cubic anharmonicity of the O-atoms optical modes. Modest cubic anharmonicity is from acoustic modes dominated by copper atoms.

Below 50 meV, the calculated broadening of phonon dispersions is not as large as the experimental phonon dispersions in Fig. 2. A previous study attributed some of the thermal behavior of cuprite to quartic anharmonicity [64]. Quartic AH contributions can account for further shifts of phonon energies. However, it does not account for phonon lineshapes. This limitation exists because the loop diagram for the quartic term does not have an imaginary part. Higher-order anharmonic processes may be needed to account for the measured thermal broadening and shifts of phonons in cuprite, so it seems challenging for perturbation theory to predict the thermal shifts of phonons in cuprite at higher temperatures.

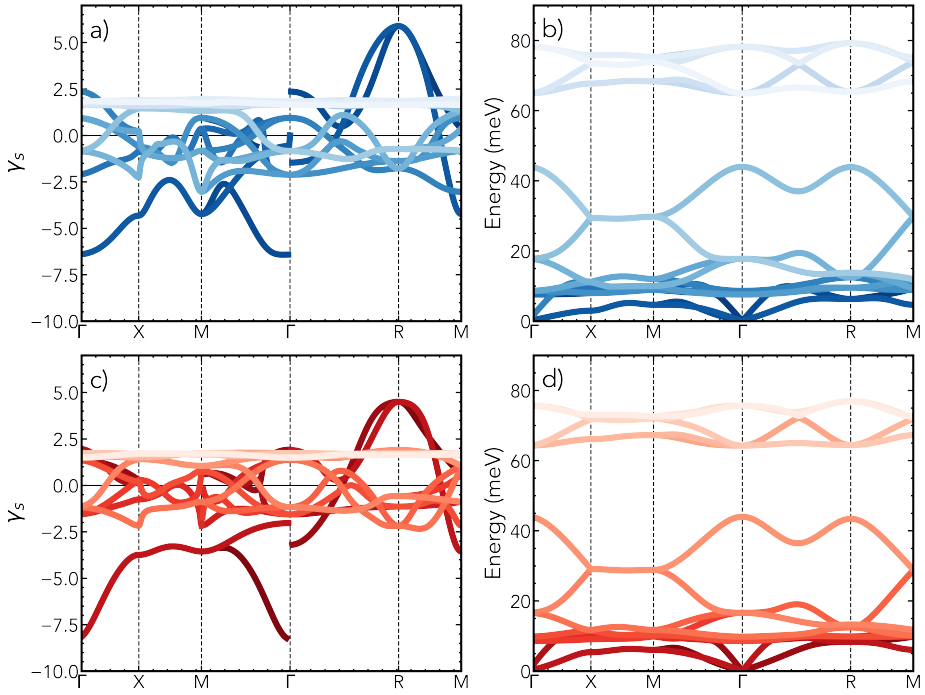

FIG. 5. Mode Grüneisen parameters for dispersions, shaded to match their corresponding dispersions at a) 10 K and c) 300 K. Phonon dispersions from quadratic terms in sTDEP calculations at b) 10 K and d) 300 K colored to correspond with their matching mode Grüneisen parameters.

VI. CONCLUSION

INS with a pulsed neutron source and an area detector with a large solid angle was used to measure all phonons in a single-crystal of cuprite at 10 K and 300 K. We directly compared phonons from QH calculations, AH calculations and experiments The AH theory better described the temperature-depend phonon trends than the QH theory. The temperature dependencies of the low-energy transverse acoustic and high-energy optical modes did not follow the experimental change in volume predicted by QH theory (which was nearly zero in QH theory since the volumes at 10 K and 300 K are nearly the same). However, calculations with AH theory predicted these shifts better than QH theory. The small negative thermal expansion in cuprite is calculated successfully with both QH and AH models. However, thermal expansion is an average over numerous phonon contributions to the Gibbs free energy. So thermal expansion may not be the best criterion for revealing the underlying thermodynamics of cuprite. The calculated AH self-energy did not capture the full thermal broadening of the measured optical modes. For cuprite, details of the measured phonon dispersions may require higher-order anharmonicity than used here.

ACKNOWLEDGMENTS

We thank Y. Shen for his insightful comments along with A. Savici for his assistance with data processing. This research used resources at the Spallation Neutron Source, a DOE Office of Science User Facility operated by the Oak Ridge National Laboratory. This work used resources from National Energy Research Scientific Computing Center (NERSC), a DOE Office of Science User Facility supported by the Office of Science of the US Department of Energy under Contract DE-AC02-05CH11231. This work was supported by the DOE Office of Science, BES, under Contract DE-FG02-03ER46055.

[1] W. Mönch, in *Semiconductor Surfaces and Interfaces* (Springer, Berlin, Heidelberg, 2001) pp. 1–20.
[2] A. Schuster, Phil. Mag. **48**, 251 (1874).
[3] Y. Abduand A. O. Musa, Rev. Mod. Phys. **2**, 8 (2009).
[4] W. H. Brattain, Rev. Mod. Phys. **23**, 203 (1951).
[5] K. Mikami, Y. Kido, Y. Akaishi, A. Quitain, and T. Kida, Sensors **19**, 1 (2019).
[6] J. Linnera, G. Sansone, L. Maschio, and A. J. Karttunen, J. Phys. Chem. C **122**, 15180 (2018).
[7] D. Y. Kim, C. W. Kim, J. H. Sohn, K. J. Lee, M. H. Jung, M. G. Kim, and Y. S. Kang, J. Phys. Chem. C **119**, 13350 (2015).
[8] M. B. Gawande, A. Goswami, F.-X. Felpin, T. Asefa, X. Huang, R. Silva, X. Zou, R. Zboril, and R. S. Varma,

Chem. Rev. **116**, 3722 (2016).
[9] L. Wan, Q. Zhou, X. Wang, T. E. Wood, L. Wang, P. N. Duchesne, J. Guo, X. Yan, M. Xia, Y. F. Li, A. A. Jelle, U. Ulmer, J. Jia, T. Li, W. Sun, and G. A. Ozin, Nat. Catal. **2**, 889898 (2019).
[10] J. Zuo, M. Kim, M. O'Keeffe, and J. Spence, Nature **401**, 4952 (1999).
[11] R. J. Elliott, Phys. Rev. **124**, 340 (1961).
[12] K. Huang, Z. Phys. **171**, 213 (1963).
[13] C. Carabatos, Phys. Status Solidi B **37**, 773 (1970).
[14] J. Hallbergand R. C. Hanso, Phys. Status Solidi B **42**, 305 (1970).
[15] G. Kugel, C. Carabatos, W. Kress, and H. Id, J. Phys. Colloques **42**, C6 (1981).
[16] Y. Petroff, P. Y. Yu, and Y. R. Shen, Phys. Rev. B **12**, 2488 (1975).
[17] A. Compaan, Solid State Commun. **16**, 293 (1975).
[18] P. Dawson, M. Hargreave, and G. Wilkinson, J. Phys. Chem. Solids **34**, 2201 (1973).
[19] J. Reydellet, M. Balkanski, and D. Trivich, Phys. Status Solidi B **52**, 175 (1972).
[20] A. Compaanand H. Z. Cummins, Phys. Rev. B **6**, 4753 (1972).
[21] P. Y. Yu, Y. R. Shen, Y. Petroff, and L. M. Falicov, Phys. Rev. Lett. **30**, 283 (1973).
[22] J. C. W. Taylorand F. L. Weichman, Can. J. Phys. **49**, 601 (1971).
[23] M. Balkanski, M. Nusimovici, and J. Reydellet, Solid State Commun. **7**, 815 (1969).
[24] E. C. Heltemes, Phys. Rev. **141**, 803 (1966).
[25] M. O'Keeffe, The Journal of Chemical Physics **39**, 1789 (1963).
[26] K. Reimannand K. Syassen, Phys. Rev. B **39**, 11113 (1989).
[27] G. K. White, J. Phys. C: Solid State Phys. **11**, 2171 (1978).
[28] W. Tiano, M. Dapiaggi, and G. Artioli, J. Appl. Crystallogr. **36**, 1461 (2003).
[29] A. Sanson, F. Rocca, G. Dalba, P. Fornasini, R. Grisenti, M. Dapiaggi, and G. Artioli, Phys. Rev. B **73**, 214305 (2006).
[30] M. Dapiaggi, W. Tiano, G. Artioli, A. Sanson, and P. Fornasini, Nucl. Instrum. Methods Phys. Res., B **200**, 231 (2003).
[31] D. L. Abernathy, M. B. Stone, M. J. Loguillo, M. S. Lucas, O. Delaire, X. Tang, J. Y. Y. Lin, and B. Fultz, Rev. Sci. Instrum. **83**, 015114 (2012).
[32] D. S. Kim, O. Hellman, J. Herriman, H. L. Smith, J. Y. Y. Lin, N. Shulumba, J. L. Niedziela, C. W. Li, D. L. Abernathy, and B. Fultz, Proc. Natl. Acad. Sci. U. S. A. **115**, 1992 (2018).
[33] P. B. Allen, Mod. Phys. Lett. B **34**, 2050025 (2020).
[34] T. Mason, D. Abernathy, I. Anderson, J. Ankner, T. Egami, G. Ehlers, A. Ekkebus, G. Granroth, M. Hagen, K. Herwig, J. Hodges, C. Hoffmann, C. Horak, L. Horton, F. Klose, J. Larese, A. Mesecar, D. Myles, J. Neuefeind, M. Ohl, C. Tulk, X.-L. Wang, and J. Zhao, Physica B Condens. **385-386**, 955 (2006).
[35] O. Arnold, J. Bilheux, J. Borreguero, A. Buts, S. Campbell, L. Chapon, M. Doucet, N. Draper, R. Ferraz Leal, M. Gigg, V. Lynch, A. Markvardsen, D. Mikkelson, R. Mikkelson, R. Miller, K. Palmen, P. Parker, G. Passos, T. Perring, P. Peterson, S. Ren, M. Reuter, A. Savici, J. Taylor, R. Taylor, R. Tolchenov, W. Zhou, and J. Zikovsky, Nucl. Instrum. Meth. A **764**, 156 (2014).
[36] J. Y. Y. Lin, F. Islam, and M. Kresh, J. Open Source Softw. **3**, 440 (2018).
[37] S. T. Omelchenko, Y. Tolstova, S. S. Wilson, H. A. Atwater, and N. S. Lewis, in *2015 IEEE 42nd Photovoltaic Specialist Conference (PVSC)* (2015) pp. 1–4.
[38] L. Y. Isseroffand E. A. Carter, Phys. Rev. B **85**, 235142 (2012).
[39] Y. Shen, C. N. Saunders, C. M. Bernal, D. L. Abernathy, M. E. Manley, and B. Fultz, Phys. Rev. Lett. **125**, 085504 (2020).
[40] M. Kresch, M. Lucas, O. Delaire, J. Y. Y. Lin, and B. Fultz, Phys. Rev. B **77**, 024301 (2008).
[41] A. Sanson, F. Rocca, G. Dalba, P. Fornasini, R. Grisenti, M. Dapiaggi, and G. Artioli, Phys. Rev. B **73**, 1 (2006).
[42] A. Wernerand H. D. Hochheimer, Phys. Rev. B **25**, 5929 (1982).
[43] V. F. Sears, Neutron News **3**, 26 (1992).
[44] M. D. Lumsden, J. L. Robertson, and M. Yethiraj, J. Appl. Crystallogr. **38**, 405 (2005).
[45] J. L. Niedziela, R. Mills, M. J. Loguillo, H. D. Skorpenske, D. Armitage, H. L. Smith, J. Y. Y. Lin, M. S. Lucas, M. B. Stone, and D. L. Abernathy, Rev. Sci. Instrum **88**, 105116 (2017).
[46] G. Kresseand J. Hafner, Phys. Rev. B **47**, 558 (1993).
[47] G. Kresseand J. Hafner, Phys. Rev. B **49**, 14251 (1994).
[48] G. Kresseand J. Furthmller, Comput. Mater. Sci. **6**, 15 (1996).
[49] G. Kresseand J. Furthmüller, Phys. Rev. B **54**, 11169 (1996).
[50] G. Kresseand D. Joubert, Phys. Rev. B **59**, 1758 (1999).
[51] J. Sun, A. Ruzsinszky, and J. P. Perdew, Phys. Rev. Lett. **115**, 036402 (2015).
[52] A. Togoand I. Tanaka, Scr. Mater. **108**, 1 (2015).
[53] O. Hellman, I. A. Abrikosov, and S. I. Simak, Phys. Rev. B **84**, 180301 (2011).
[54] O. Hellman, P. Steneteg, I. A. Abrikosov, and S. I. Simak, Phys. Rev. B **87**, 104111 (2013).
[55] O. Hellmanand I. A. Abrikosov, Phys. Rev. B **88**, 144301 (2013).
[56] T. H. K. Barronand M. L. Klein, Perturbation theory of anharmonic crystals, in *Dynamical Properties of Solids*, edited by G. Hortonand A. Maradudin (North-Holland, Amsterdam, 1974) p. 391.
[57] A. A. Maradudinand A. E. Fein, Phys. Rev. **128**, 2589 (1962).
[58] D. C. Wallace, *Statistical Physics of Crystals and Liquids* (World Scientific, 2003).
[59] J. Linnera, A. Erba, and A. J. Karttunen, J. Chem. Phys. **151**, 184109 (2019).
[60] W. Schäferand A. Kirfel, Appl. Phys. A **74**, s1010s1012 (2002).
[61] K.-P. Bohnen, R. Heid, L. Pintschovius, A. Soon, and C. Stampfl, Phys. Rev. B **80**, 134304 (2009).
[62] R. Mittal, S. L. Chaplot, S. K. Mishra, and P. P. Bose, Phys. Rev. B **75**, 174303 (2007).
[63] L. H. Rimmer, M. T. Dove, B. Winkler, D. J. Wilson, K. Refson, and A. L. Goodwin, Phys. Rev. B **89**, 28 (2014).
[64] M. K. Gupta, R. Mittal, S. L. Chaplot, and S. Rols, J. Appl. Phys. **115**, 093507 (2014).
[65] M. M. Begand S. M. Shapiro, Phys. Rev. B **13**, 1728 (1976).

[66] E. T. Ritz, S. J. Li, and N. A. Benedek, J. Appl. Phys **126**, 171102 (2019).

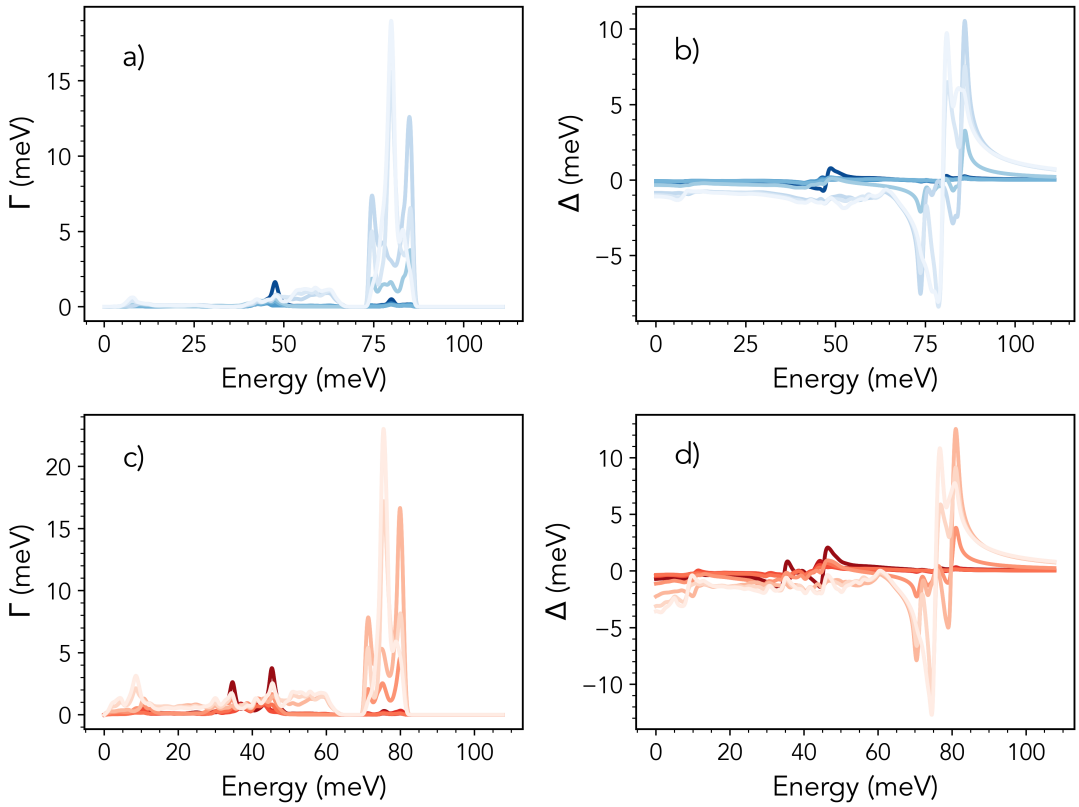

FIG. 6. The imaginary part (Γ) of the phonon self-energy at a) 10 K in blue and c) 300 K shown in red. Different shades of red and blue correspond to individual modes designated by Figs. 5b, d) for the real part (Δ) of the phonon self-energy. Data are for $\vec{Q} = (0.25, 025, 0.0)$.

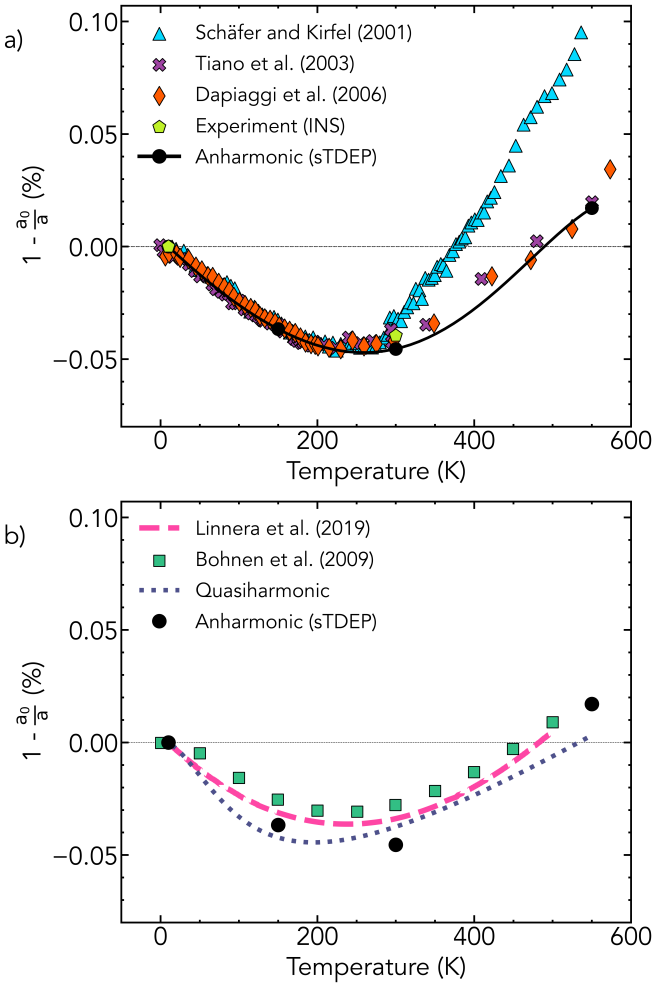

FIG. 7. Percentage change with temperature of lattice parameter of cuprite from experiment and computation. a) Experimental results [28–30, 60] are shown as colored markers, compared to AH result from minimized free energies using sTDEP. b) Calculated percentage change of lattice parameter versus temperature. QH results are colored line and markers [59, 61], compared to sTDEP results shown with black circles.